VIP Organized Nanotubes Very Important Paper

DOI: 10.1002/ange.201307256

Ionic Self-Assembly Provides Dense Arrays of Individualized, Aligned Single-Walled Carbon Nanotubes**

*Jean-Hubert Olivier, Pravas Deria, Jaehong Park, Amar Kumbhar, Maria Andrian-Albescu, and Michael J. Therien**

Single-walled carbon nanotubes (SWNTs) stand among the most studied nanomaterials owing to their uncommon mechanical, optical, electrical, magnetic, and thermal properties, which make them ideal components and building blocks for a wide range of devices and materials.[1] The development of many such SWNT-based devices and materials underscores the need for solvent-dispersed SWNTs. Modified nanotubes are thus required to circumvent the strong tendency of these nanostructures to aggregate and precipitate. As the preservation of many of the unique physical and optoelectronic properties of SWNTs necessitates undisrupted nanotube conjugation, development of versatile noncovalent solubilization and organization strategies are essential.

Conjugated polymers have been exploited to provide stable polymer–SWNT dispersions in organic solvent.[2] We have shown previously that the use of a phase-transfer catalyst enables highly charged [arylene]ethynylene polymers, such as poly[2,6-{1,5-bis(3-propoxysulfonicacidsodium-salt)}naphthylene]ethynylene (PNES), to exfoliate and individualize SWNTs in organic solvents;[3] these organic-solvent suspended SWNTs demonstrate a self-assembled superstructure in which an anionic [arylene]ethynylene polymer monolayer helically wraps the nanotube surface at periodic and constant morphology (Scheme 1 a); extensive AFM and TEM data demonstrate a persistent [arylene]ethynylene polymer–SWNT superstructure regardless of solvent.[3] Such single chain, monolayer wrapping minimizes the polymer:SWNT molar ratio of the organic-solvent soluble SWNT composition. While these polymer–SWNT compositions uniquely enable wide-ranging SWNT solubility, these initial designs do not provide a means to organize SWNTs in the solid state.

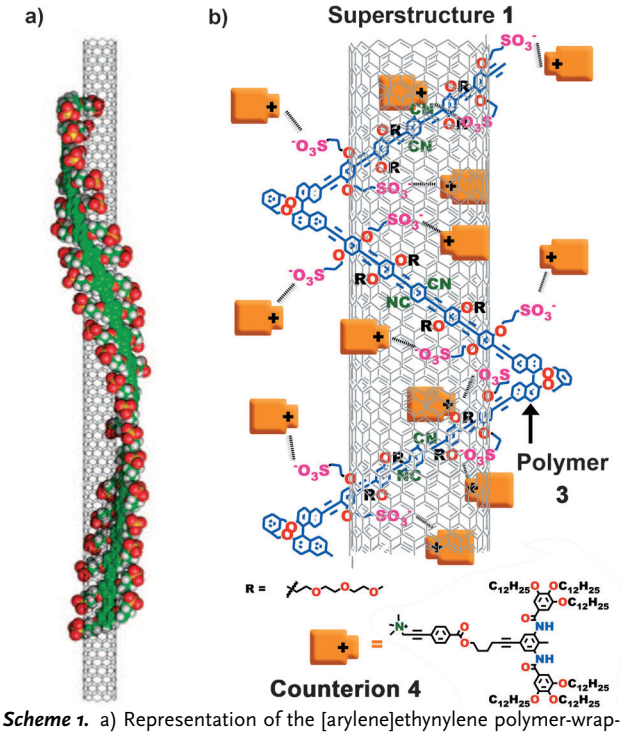

Scheme 1. a) Representation of the [arylene]ethynylene polymer-wrapped SWNT. b) Representation of the ionic self-assembled nanostructure **1** showing the molecular formulas of the anionic conjugated polymer **3** and the amphiphilic cation **4**.

Developing the means to control SWNT organization in multi-component ensembles has been a long-standing goal. Herein we demonstrate that polyanionic [arylene]ethynylene polymers, designed to helically wrap SWNTs (Supporting Information), used in combination with ionic self-assembly (ISA) approaches and nanotubes enriched in the (6,5) chirality, enable for the first time the production of functionalized SWNTs that are: 1) fully soluble in organic solvents, and 2) capable of assembly into complex hierarchical structures that feature aligned nanotubes that maintain the optoelectronic properties characteristic of individualized SWNTs.

The combination of high aspect ratio and substantial intertube van der Waals interactions makes difficult the development of solid-state materials that feature aligned, yet individualized SWNTs. Approaches developed toward this goal have included: 1) doping aqueous solutions of dispersed SWNTs[4] into pre-existing lyotropic or thermotropic liquid crystals,[5] 2) exploiting SWNT interactions with ionic liquids,[6] organic molecules,[7] or polymers[8] to drive formation of composite gels, and 3) post-processing methods that have

[*] Dr. J.-H. Olivier, Dr. P. Deria, Dr. J. Park, M. Andrian-Albescu, Prof. M. J. Therien
Department of Chemistry, Duke University
French Family Science Center
124 Science Drive, Durham, North Carolina 27708 (USA)
E-mail: michael.therien@duke.edu
Homepage: http://www.chem.duke.edu/~mt83/
Dr. A. Kumbhar
Chapel Hill Analytical & Nanofabrication Laboratory
University of North Carolina at Chapel Hill
243 Chapman Hall, NC 27599 (USA)

[**] This work was funded by the Division of Chemical Sciences, Geosciences, and Biosciences, Office of Basic Energy Sciences, of the U.S. Department of Energy through Grant DE-SC0001517. Infrastructural support was provided by the NSEC (DMR-0425780) program of the National Science Foundation.

Supporting information for this article is available on the WWW under http://dx.doi.org/10.1002/anie.201307256.

relied, for example, on external electric,[9] or magnetic fields.[10] In these SWNT-containing solid-state materials, a significant fraction of individualized nanotubes is only realized when the SWNT mass fraction is low (typically $<5\%$). SWNTs wrapped with chiral polyanionic [arylene]ethynylene polymers, however, make possible for the first time the use of ISA approaches to derive solid-state SWNT materials from solution that feature aligned, individualized nanotubes at high mass fraction.

ISA has emerged as a powerful tool to create new nanostructures and functional materials by coupling oppositely charged building blocks through electrostatic attraction;[11] for example, both polyelectrolytes and oligoelectrolytes have been used as ISA building blocks to produce electrochemically active mesormorphous structures[12] and liquid-crystalline materials.[13] ISA approaches have never been applied to the development of carbon nanotube materials, owing to the lack of robust functionalized SWNTs that feature charged moieties arrayed about the nanotube surface in a periodic and homogeneous fashion. SWNTs that are single-chain helically wrapped by highly charged anionic [arylene]ethynylene polymers,[14] however, define ISA compatible nanostructures.[3] We report herein that the conjugated anionic polymer **3** (Scheme 1b), which incorporates an asymmetric binaphthalene unit as an integral component of its π-conjugated repeat unit, used in combination with the bulky, paraffinic cation **4** (Scheme 1b), make the ISA of SWNTs possible. Using methods described previously, **3** was utilized to wrap (6,5) SWNTs;[15] established gel permeation chromatography (GPC) purification methods show that **3**:SWNT superstructures (**2**), in which the nanotube is helically wrapped by polyanionic polymer **3**, feature no measurable concentration of uncomplexed **3** (Scheme S4; Figure S7). Statistical analyses of AFM data establish an average (6,5) SWNT length of 700 ± 50 nm in these samples (Figure S8).

The **3**:SWNT superstructure **2** can be transferred from aqueous solution to a 1:1 DMSO:MeOH solvent mixture by utilizing 15-crown-5 as a phase-transfer agent;[3] the ionic self-assembled nanostructure, **1** (Scheme 1b) was formed through a metathesis reaction (Scheme S4) of **2** with the elaborated amphiphilic cation **4**. Note that the structure of the amphiphilic cation **4**, will play a pivotal role in directing hierarchical organization of **1** units in the solid state, and features hydrogen-bonding amide and paraffinic side-chain components. Although related amphiphilic structures have been utilized, for example, to generate luminescent liquid crystals,[16] note that **4** features topological flexibility between the ammonium cation and the amide linkage groups: this design promotes hydrogen-bonding and hydrophobic interactions between neighboring **4** units that decorate the anionic polymer-wrapped nanotube module (see IR spectroscopic data, Figure S4).

A Vis-NIR absorption spectrum of **1** (that is, the **3**-wrapped [(6,5) SWNT] that has **4** as counterions) in THF solvent is displayed in Figure 1; note that this spectrum is essentially the same as that acquired for **2** in 3:7 MeOH:D_2O, indicating that the electronic properties of the self-assembled hybrid **1**, derived from ISA, is not perturbed relative to **2**.

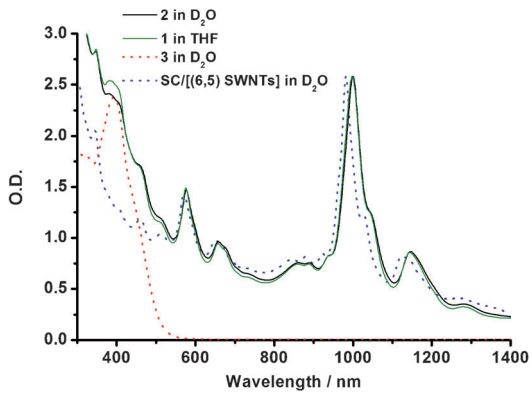

Figure 1. Electronic absorption spectra of: **2** in 3:7 MeOH:-D_2O (black); **1** in THF solvent (green); **3** in 3:7 MeOH:D_2O (dashed orange); and aqueous sodium cholate suspension of (6,5) SWNTs (SC-[(6,5) SWNTs]) (dashed blue).

Modest bathochromic shifts of the E_{11} and E_{22} transitions (ca. 173 cm^{-1}) of THF-suspended **1** relative to the analogous spectrum recorded for benchmark aqueous sodium cholate suspensions of (6,5) SWNTs (SC-[(6,5) SWNTs]) are observed: previous work suggests that such spectral shifts derive in large part from changes in solvent polarity and electrophilicity, and variations in the extent to which SWNTs are solvated in these types of samples.[17]

Experimental evaluation of the degree to which the nanotube surface is covered by the semiconducting polyelectrolyte can be determined from the **1** polymer:nanotube molar ratio and the helical pitch length (Supporting Information). Considering an average SWNT length of 700 nm and an observed helical pitch length of 9 ± 2 nm determined from AFM data (Figure S6), approximately 250 polymer repeat units cover the nanotube surface. These results suggest that the helical pitch length corresponds to 21 aromatic units (3.5 polymer repeat units), indicating that approximately 20% of nanotube surface is covered by the conjugated polymer backbone. Previously reported MD simulations that examined poly[*p*-{2,5-bis(3-propoxysulfonicacidsodiumsalt)}-phenylene]ethynylene-wrapped SWNTs (PPES-SWNTs) establish a helical pitch length of 14 ± 1 nm, and a polymer–nanotube surface coverage of approximately 11%.[18]

The elemental composition of a **1**-based thin film was investigated by X-ray photoelectron spectroscopy (XPS; Figure S3) and demonstrates an electrostatic interaction of one sulfonate group with one amphiphilic cation **4**, highlighting the completeness of the metathesis reaction. AFM experiments were utilized to probe the structure of the parent supramolecular polyelectrolyte **2**, and that of the hybrid composition **1** derived from ISA. As shown Figure 2a, no entangled structures can be detected in the aqueous **2** sample. Topographic AFM shows that the height profile of these individualized polymer-wrapped SWNTs ranges from 0.9 to 1.3 nm. Given that the (6,5) SWNT diameter is 0.7 nm, this height-profile analysis confirms that samples of **2** in aqueous solvent are composed of individualized carbon nanotubes. In contrast, identical experiments that examine **1** in MeOH:THF solvent (Figure 2b) highlight both entangled tubes and

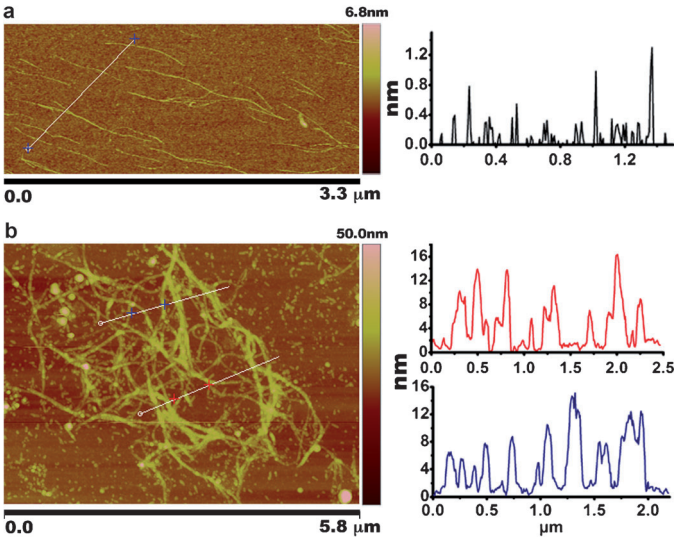

Figure 2. Topographic (tapping mode) AFM images and corresponding height profile of: a) **2** dropcast from an aqueous suspension on a Si surface, and b) **1** dropcast from a 3:7 MeOH:THF solution on a Si surface.

a fibrous-like morphology. A corresponding height profile analysis reveals the existence of structures that range in diameter from 4 to 16 ± 1 nm, congruent with the expectation that uniform incorporation of the amphiphilic cation **4** following metathesis should dramatically increase the overall diameter of the resulting nanostructure. Species that exhibit a 4 nm diameter are thus assigned to individualized **1** superstructures, whereas larger assemblies correspond to small fibers built from interactions of the paraffinic **4** counterions that decorate individualized tubes.

Differential scanning calorimetry (DSC) was utilized to probe any temperature-dependent phase transitions of **1**. Initial heating of a **1**-based thin film shows a DSC trace that highlights a non-reversible endothermic transition that occurs over a 20–90 °C temperature range, with two peaks at 53 and 83 °C (Figure 3a). The irreversible nature of this transition indicates that ambient temperature precipitation of **1** gives rise to a metastable state that is destabilized at high temperature. Re-dispersion of **1** heated in this manner cannot be achieved in any solvent, even after long periods of sonication, suggesting that heating induces a drastic structural change. A SEM image of the ionic self-assembled nanostructure **1** prior to thermal treatment (Figure 3b) highlights a porous material derived from a fibrous SWNT network. Figure 3c, in contrast, emphasizes the radical change in morphology that this **1** sample undergoes upon heating: the resulting amorphous material is clearly non-porous. These experiments indicate that thermal activation does not drive formation of an organized state, as observed for thermotropic liquid-crystalline materials, but rather disrupts the initial structured morphology. This behavior likely derives at least in part from the high SWNT aspect ratio, suggesting that the supramolecular polyelectrolyte **1**, based on 700 nm long SWNTs, lacks the requisite nanostructural flexibility in the solid-state network to achieve anisotropic stabilization (for more details, see Figure S17 and related discussion).

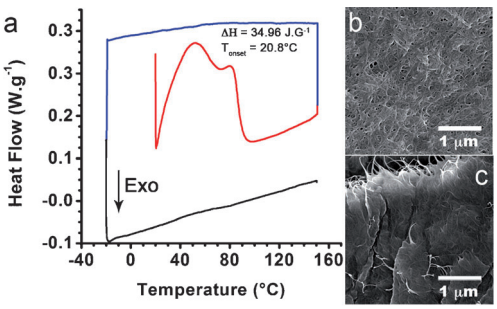

Figure 3. a) DSC traces of **1** obtained at a scan rate of 10 °C min^{-1}: (red) first heating cycle, (blue) first cooling cycle, (black) second heating cycle. b) SEM images of **1** prior to thermal treatment, and c) after heating at 120 °C for 5 min.

The excellent solubility of **1** in low-boiling point solvents, such as THF (1.4 mg mL^{-1}), facilitates manipulation of this SWNT-based supramolecular polyelectrolyte into both amorphous thin films of uniform thickness and ordered assemblies. Simple spin coating onto hydroxy- and alkyl-functionalized silicon wafer surfaces provides thin films having homogeneously thick carbon nanotube layers; spinning rates of 6000 and 4000 rpm provide, respectively, film thicknesses of 50 and 100 nm (Supporting Information). As depicted in Figure S9, a uniform network of randomly distributed carbon nanotubes is realized in each case. In contrast, macroscopic structures that feature varying degrees of nanotube–nanotube mutual orientation can be realized though manipulation of the **1** solvation environment (Figure 4). In contrast to the morphology derived from the metathesis reaction and subsequent precipitation that produces **1** (Figure 4a), injection of a THF solution of **1** (500 µL; concentration = 1.4 mg mL^{-1}) into DMSO (20 mL) drives rapid formation of a unidirectional network composed of interacting organic fibers (OFs) (Figure 4c); Figure 4b highlights the genesis of these organic fibers, showing how individual **1** fibrils merge to form larger fibrous structures. Under these experimental conditions, the size domains of these continuous compact superstructures shown in Figure 4c range from 2–50 µm in length and 0.5–2.0 µm in width. Compared to the fast nucleation of fibrous structures realized through direct solvent injection, the macroscopic assemblies generated by slow solvent diffusion display a significantly greater degree of order (Figure 4d–h). Slow diffusion of methanol or nitromethane into THF solutions of **1** over a period of several days results in the formation of a gelatinous material that does not flow under gravity (Figure S11). These gel materials are composed of ribbon-like structures that are stable over a period of months, and exhibit no sign of collapse or precipitation. These highly ordered materials derived from **1** immobilize solvent (the defining property of a gel) within an organized 3D network made possible by the counterion **4**. Polarized optical micrographs of these assemblies show a birefringent texture, indicating significant anisotropic organization of these SWNT-based fibers (Figure S12). SEM images of a dried sample of these SWNT-based ribbon

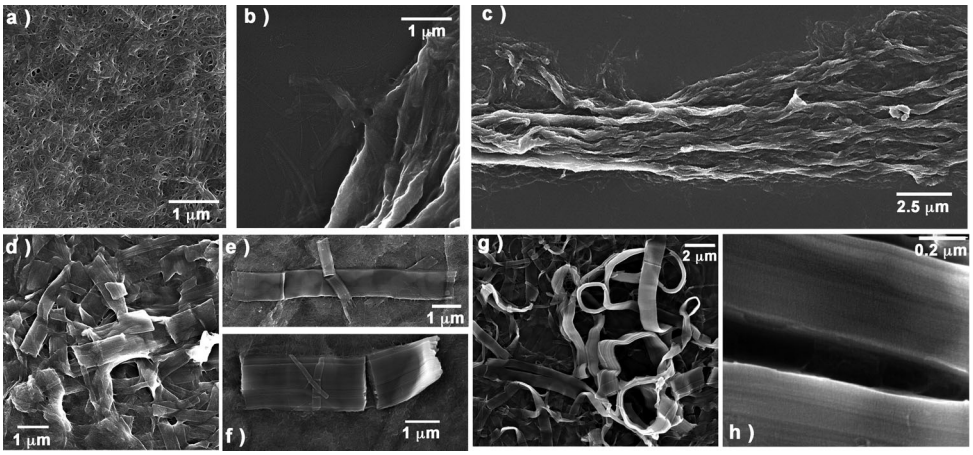

Figure 4. Scanning electron microscopic (SEM) images of a) The **1** precipitate produced following metathesis of **2** with **4**. b,c) Fibers formed following fast injection of a THF solution of **1** into DMSO. d) Aligned **1** domains produced by slow diffusion of $MeNO_2$ into a THF solution of **1**. e–h) Aligned **1** ribbons produced through slow diffusion of MeOH into a **1** THF solution. e, f) **1** ribbons; g) **1** ribbons of lengths that range up to 30 μm. h) Enlarged view of the ribbons displayed in (g) that highlights the remarkable degree of SWNT alignment that characterizes these structures.

structures prepared by $MeNO_2$ diffusion into THF (Figure 4 d) are congruent with the sample's original gel-like nature, highlighting that a porous SWNT fiber network results from shrinkage and loss of trapped solvent during the drying process. The most compelling aspect of these ribbon-like structures emphasized in the Figure 4 d–h images is the extraordinary compact architecture characterized by the seemingly perfect parallel alignment of SWNT-based fibers (Figure 4 h). The length domain of these **1** ribbons ranges from a few micrometers (Figure 4 f,g) to several tens of micrometers (Figure 4 e–g), with corresponding widths and thicknesses varying respectively between 0.5–2 μm and 0.2–0.3 μm. As the thickness of an individualized **1** is approximately 4 nm (see above), these 0.5–2 μm-wide ribbons are composed of approximately 125–500 aligned SWNTs. These samples thus feature perfectly aligned SWNTs at high areal density (2.5×10^{10} SWNTs cm^{-2}). This areal density exceeds that thought necessary (1.0×10^{10} SWNTs cm^{-2}) for the development of SWNT-transistor-based high-performance logic circuits,[19] and is rivaled only by the areal density of SWNT arrays assembled by the Langmuir–Schaefer method.[20] It is important to note in this respect, however, that the aligned nanotubes of Figure 4 d–h feature electro-optically isolated individual SWNTs, as each nanotube component of these ribbons is helically wrapped by a highly charged polymer. These highly aligned, high nanotube areal density **1**-based ribbons, made possible by the combination of left-handed helical wrapping of the SWNT by the polyanionic polymer **3** and the amphiphilic nature of the **4** cation, underscore the appeal and potential of this solution-phase approach to post-process carbon nanotubes and create unique hybrid semiconducting polymer-SWNT architectures.

Figure S16a displays the solid-state electronic absorption spectrum of these **1**-based ribbons relative to that obtained for a dilute **1** THF solution. Note that these solid-state and solution spectra are identical: no spectral shifting is evident for the distinct Van Hove transitions (E_{11}: 999 nm; E_{22}: 576 nm; E_{33}: 378 nm) of (6,5) tubes. Figure S16b displays the dependence of transmitted, polarized light ($\lambda=$ 1000 nm) for a drop cast **1** film and **1**-based ribbons (Figure 4 d) on quartz slides as a function of the incident beam polarization angle. As E_{11} excitation gives rise to a SWNT transition polarized along the nanotube longitudinal axis,[21] the light transmitted at 1000 nm for a fixed (6,5) SWNT concentration is inversely proportional to the SWNT population collinear with incident beam polarization.[4e] While it is important to note that the spot size of the incident beam (180 μm) exceeds the dimensions of the longest **1**-based ribbons (ca. 100 μm), it is clear that the drop-cast sample features randomly oriented SWNTs, while the ribbon structures exhibit a strong dependence of transmittance with incident beam polarization angle. These optical experiments chronicled in Figure S16 corroborate the individualized and insulated nature of the SWNTs that compose these dried **1** gels, and underscore the exceptional SWNT order enabled by ISA of superstructure **2** with cation **4** and subsequent diffusion-controlled precipitation.

This work shows that chiral polyanionic [arylene]ethynylene polymers that helically wrap SWNTs, used in combination with ionic self-assembly (ISA) approaches, enable for the first time the production of functionalized SWNTs that are both fully soluble in organic solvents, and capable of assembly into complex hierarchical structures that feature aligned nanotubes that maintain their respective individualized character. Combined atomic force microscopy and spectroscopic investigations of these assemblies reveal fibrous structures derived from aligned individualized SWNTs. Modulation of the precipitation conditions produces gels in which SWNTs, helically wrapped by chiral [arylene]ethynylene polymers, self-organize into highly aligned domains (ribbon structures) that span several tens of micrometers in length. Remarkably, these macroscopic networks composed of rigorously aligned, closely packed SWNTs (Figure 4 h) feature individualized nanotube densities as high as 2.5×10^{10} cm^{-2}, exceeding the threshold thought necessary to realize SWNT-based high performance logic elements;[19] moreover, as this ISA approach relies upon SWNTs that are helically wrapped by a highly charged polymer, these aligned assemblies feature electro-optically isolated SWNTs. This ionic self-assembly approach to SWNT organization thus offers an appealing alternative to traditional SWNT alignment methods that include horizontal SWNT growth on a single-crystal surface[22] or chemical vapor deposition under gas flow,[23] because ISA

1) is a solution-based process, and 2) provides complex hierarchical SWNT structures based on fixed stoichiometry/fixed morphology SWNT-polymer compositions. We suggest that the combination of chiral polyanionic [arylene]ethynylene polymers, SWNTs having electronic structural homogeneity,[24] the ability to modulate polymer electronic structure by design, and the facility of ISA to provide hierarchical organization, offers exceptional promise for the development of new types of electro-optic materials.

Received: August 18, 2013
Published online: October 15, 2013

Keywords: carbon nanotubes · hybrid nanomaterial · ionic self-assembly · polyanionic polymers

[1] a) D. M. Guldi, N. Martín, *Carbon Nanotubes and Related Structures: Synthesis Characterization, Functionalization, and Applications*, VCH, Weinheim, **2010**; b) M. A. O'Connel, *Carbon Nanotubes: Properties and Applications*, Taylor and Francis, Boca Raton, **2006**; c) S. Reich, C. Thomsen, J. Maultzsch, *Carbon Nanotubes*, VCH, Weinheim, **2004**; d) K. Liu, J. Deslippe, F. Xiao, R. B. Capaz, X. Hong, S. Aloni, A. Zettl, W. Wang, X. Bai, S. G. Louie, E. Wang, F. Wang, *Nat. Nanotechnol.* **2012**, *7*, 325 – 329; e) Q. Cao, J. A. Rogers, *Adv. Mater.* **2009**, *21*, 29 – 53; f) L. J. Carlson, T. D. Krauss, *Acc. Chem. Res.* **2008**, *41*, 235 – 243; g) P. Avouris, M. Freitag, V. Perebeinos, *Nat. Photonics* **2008**, *2*, 341 – 350; h) S. Kilina, S. Tretiak, *Adv. Funct. Mater.* **2007**, *17*, 3405 – 3420; i) D. R. Kauffman, A. Star, *Small* **2007**, *3*, 1324 – 1329.

[2] a) F. Lemasson, N. Berton, J. Tittmann, F. Hennrich, M. M. Kappes, M. Mayor, *Macromolecules* **2011**, *45*, 713 – 722; b) H. W. Lee, Y. Yoon, S. Park, J. H. Oh, S. Hong, L. S. Liyanage, H. Wang, S. Morishita, N. Patil, Y. J. Park, J. J. Park, A. Spakowitz, G. Galli, F. Gygi, P. H. S. Wong, J. B. H. Tok, J. M. Kim, Z. Bao, *Nat. Commun.* **2011**, *2*, 541; c) P. Imin, M. Imit, A. Adronov, *Macromolecules* **2011**, *44*, 9138 – 9145; d) J.-Y. Hwang, A. Nish, J. Doig, S. Douven, C.-W. Chen, L.-C. Chen, R. J. Nicholas, *J. Am. Chem. Soc.* **2008**, *130*, 3543 – 3553; e) D. A. Walters, M. J. Casavant, X. C. Qin, C. B. Huffman, P. J. Boul, L. M. Ericson, E. H. Haroz, M. J. O'Connell, K. Smith, D. T. Colbert, R. E. Smalley, *Chem. Phys. Lett.* **2001**, *338*, 14 – 20.

[3] P. Deria, L. E. Sinks, T.-H. Park, D. M. Tomezsko, M. J. Brukman, D. A. Bonnell, M. J. Therien, *Nano Lett.* **2010**, *10*, 4192 – 4199.

[4] a) W. Song, I. A. Kinloch, A. H. Windle, *Science* **2003**, *302*, 1363 – 1364; b) V. A. Davis, L. M. Ericson, A. N. G. Parra-Vasquez, H. Fan, Y. Wang, V. Prieto, J. A. Longoria, S. Ramesh, R. K. Saini, C. Kittrell, W. E. Billups, W. W. Adams, R. H. Hauge, R. E. Smalley, M. Pasquali, *Macromolecules* **2004**, *37*, 154 – 160; c) P. K. Rai, R. A. Pinnick, A. N. G. Parra-Vasquez, V. A. Davis, H. K. Schmidt, R. H. Hauge, R. E. Smalley, M. Pasquali, *J. Am. Chem. Soc.* **2006**, *128*, 591 – 595; d) V. Weiss, R. Thiruvengadathan, O. Regev, *Langmuir* **2006**, *22*, 854 – 856; e) C. Zamora-Ledezma, C. Blanc, M. Maugey, C. Zakri, P. Poulin, E. Anglaret, *Nano Lett.* **2008**, *8*, 4103 – 4107; f) V. A. Davis, A. N. G. Parra-Vasquez, M. J. Green, P. K. Rai, N. Behabtu, V. Prieto, R. D. Booker, J. Schmidt, E. Kesselman, W. Zhou, H. Fan, W. W. Adams, R. H. Hauge, J. E. Fischer, Y. Cohen, Y. Talmon, R. E. Smalley, M. Pasquali, *Nat. Nanotechnol.* **2009**, *4*, 830 – 834; g) X. Xin, H. Li, S. A. Wieczorek, T. Szymborski, E. Kalwarczyk, N. Ziebacz, E. Gorecka, D. Pociecha, R. Holyst, *Langmuir* **2010**, *26*, 3562 – 3568; h) N. Puech, C. Blanc, E. Grelet, C. Zamora-Ledezma, M. Maugey, C. Zakri, E. Anglaret, P. Poulin, *J. Phys. Chem. C* **2011**, *115*, 3272 – 3278.

[5] a) S. Bhattacharyya, J.-P. Salvetat, D. Roy, V. Heresanu, P. Launois, M.-L. Saboungi, *Chem. Commun.* **2007**, 4248 – 4250; b) H. K. Bisoyi, S. Kumar, *J. Mater. Chem.* **2008**, *18*, 3032 – 3039; c) G. Scalia, C. von Bühler, C. Hägele, S. Roth, F. Giesselmann, J. P. F. Lagerwall, *Soft Matter* **2008**, *4*, 570 – 576; d) M. Kimura, N. Miki, N. Adachi, Y. Tatewaki, K. Ohta, H. Shirai, *J. Mater. Chem.* **2009**, *19*, 1086 – 1092; e) H. W. Lee, W. You, S. Barman, S. Hellstrom, M. C. LeMieux, J. H. Oh, S. Liu, T. Fujiwara, W. M. Wang, B. Chen, Y. W. Jin, J. M. Kim, Z. Bao, *Small* **2009**, *5*, 1019 – 1024; f) K. Okano, I. Noguchi, T. Yamashita, *Macromolecules* **2010**, *43*, 5496 – 5499; g) G. Ao, D. Nepal, M. Aono, V. A. Davis, *ACS Nano* **2011**, *5*, 1450 – 1458; h) S. Zhang, S. Kumar, *Small* **2008**, *4*, 1270 – 1283.

[6] a) T. Fukushima, T. Aida, *Chem. Eur. J.* **2007**, *13*, 5048 – 5058; b) T. Fukushima, A. Kosaka, Y. Ishimura, T. Yamamoto, T. Takigawa, N. Ishii, T. Aida, *Science* **2003**, *300*, 2072 – 2074.

[7] a) T. Ogoshi, Y. Takashima, H. Yamaguchi, A. Harada, *J. Am. Chem. Soc.* **2007**, *129*, 4878 – 4879; b) M. S. Arnold, M. O. Guler, M. C. Hersam, S. I. Stupp, *Langmuir* **2005**, *21*, 4705 – 4709; c) F. G. Brunetti, C. Romero-Nieto, J. López-Andarias, C. Atienza, J. L. López, D. M. Guldi, N. Martín, *Angew. Chem.* **2013**, *125*, 2236 – 2240; *Angew. Chem. Int. Ed.* **2013**, *52*, 2180 – 2184; d) C. Romero-Nieto, R. García, M. Á. Herranz, C. Ehli, M. Ruppert, A. Hirsch, D. M. Guldi, N. Martín, *J. Am. Chem. Soc.* **2012**, *134*, 9183 – 9192.

[8] a) S. Srinivasan, S. S. Babu, V. K. Praveen, A. Ajayaghosh, *Angew. Chem.* **2008**, *120*, 5830 – 5833; *Angew. Chem. Int. Ed.* **2008**, *47*, 5746 – 5749; b) E. Cheng, Y. Li, Z. Yang, Z. Deng, D. Liu, *Chem. Commun.* **2011**, *47*, 5545 – 5547; c) J. Chen, C. Xue, R. Ramasubramaniam, H. Liu, *Carbon* **2006**, *44*, 2142 – 2146; d) A. B. Schoch, K. R. Shull, C. L. Brinson, *Macromolecules* **2008**, *41*, 4340 – 4346.

[9] X. Q. Chen, T. Saito, H. Yamada, K. Matsushige, *Appl. Phys. Lett.* **2001**, *78*, 3714 – 3716.

[10] J. Hone, M. C. Llaguno, N. M. Nemes, A. T. Johnson, J. E. Fischer, D. A. Walters, M. J. Casavant, J. Schmidt, R. E. Smalley, *Appl. Phys. Lett.* **2000**, *77*, 666 – 668.

[11] C. F. J. Faul, M. Antonietti, *Adv. Mater.* **2003**, *15*, 673 – 683.

[12] Z. Wei, T. Laitinen, B. Smarsly, O. Ikkala, C. F. J. Faul, *Angew. Chem.* **2005**, *117*, 761 – 766; *Angew. Chem. Int. Ed.* **2005**, *44*, 751 – 756.

[13] a) J.-H. Olivier, F. Camerel, G. Ulrich, J. Barberá, R. Ziessel, *Chem. Eur. J.* **2010**, *16*, 7134 – 7142; b) F. Camerel, J. Barberá, J. Otsuki, T. Tokimoto, Y. Shimazaki, L.-Y. Chen, S.-H. Liu, M.-S. Lin, C.-C. Wu, R. Ziessel, *Adv. Mater.* **2008**, *20*, 3462 – 3467; c) J. Kadam, C. F. J. Faul, U. Scherf, *Chem. Mater.* **2004**, *16*, 3867 – 3871.

[14] H. Jiang, P. Taranekar, J. R. Reynolds, K. S. Schanze, *Angew. Chem.* **2009**, *121*, 4364 – 4381; *Angew. Chem. Int. Ed.* **2009**, *48*, 4300 – 4316.

[15] J. Park, P. Deria, M. J. Therien, *J. Am. Chem. Soc.* **2011**, *133*, 17156 – 17159.

[16] a) S. Frein, F. Camerel, R. Ziessel, J. Barbera, R. Deschenaux, *Chem. Mater.* **2009**, *21*, 3950 – 3959; b) F. Camerel, R. Ziessel, B. Donnio, C. Bourgogne, D. Guillon, M. Schmutz, C. Iacovita, J. P. Bucher, *Angew. Chem.* **2007**, *119*, 2713 – 2716; *Angew. Chem. Int. Ed.* **2007**, *46*, 2659 – 2662; c) F. Camerel, L. Bonardi, M. Schmutz, R. Ziessel, *J. Am. Chem. Soc.* **2006**, *128*, 4548 – 4549.

[17] B. A. Larsen, P. Deria, J. M. Holt, I. N. Stanton, M. J. Heben, M. J. Therien, J. L. Blackburn, *J. Am. Chem. Soc.* **2012**, *134*, 12485 – 12491.

[18] Y. K. Kang, O.-S. Lee, P. Deria, S. H. Kim, T.-H. Park, D. A. Bonnell, J. G. Saven, M. J. Therien, *Nano Lett.* **2009**, *9*, 1414 – 1418.

[19] a) A. D. Franklin, M. Luisier, S.-J. Han, G. Tulevski, C. M. Breslin, L. Gignac, M. S. Lundstrom, W. Haensch, *Nano Lett.* **2012**, *12*, 758 – 762; b) N. Patil, J. Deng, M. Mitra H.-S. P. Wong, *IEEE Trans. Nanotechnol.* **2009**, *8*, 37 – 45.
[20] Q. Cao, S.-j. Han, G. S. Tulevski, Y. Zhu, D. D. Lu, W. Haensh, *Nat. Nanotechnol.* **2013**, *8*, 180 – 186.
[21] S. Kilina, S. Tretiak, S. K. Doorn, Z. Luo, F. Papadimitrakopoulos, A. Piryatinski, A. Saxena, A. R. Bishop, *Proc. Natl. Acad. Sci. USA* **2008**, *105*, 6797 – 6802.
[22] a) C. Kocabas, S. H. Hur, A. Gaur, M. A. Meitl, M. Shim, J. A. Rogers, *Small* **2005**, *1*, 1110 – 1116; b) A. Ismach, L. Segev, E. Wachtel, E. Joselevich, *Angew. Chem.* **2004**, *116*, 6266 – 6269; *Angew. Chem. Int. Ed.* **2004**, *43*, 6140 – 6143.
[23] a) S. Huang, B. Maynor, X. Cai, J. Liu, *Adv. Mater.* **2003**, *15*, 1651 – 1655; b) L. X. Zheng, M. J. O'Connel, S. K. Doorn, X. Z. Liao, Y. H. Zhao, E. A. Akhadov, M. A. Hoffbauer, B. J. Roop, Q. X. Jia, R. C. Dye, D. E. Peterson, S. M. Huang, J. Liu, Y. T. Zhu, *Nat. Mater.* **2004**, *3*, 673 – 676.
[24] M. S. Arnold, A. A. Green, J. F. Hulvat, S. I. Stupp, M. C. Hersam, *Nat. Nanotechnol.* **2006**, *1*, 60 – 65.

